NANO LETTERS

2009
Vol. 9, No. 5
2077-2082

A Nanocube Plasmonic Sensor for Molecular Binding on Membrane Surfaces

William J. Galush,[†,‡] Sarah A. Shelby,[§] Martin J. Mulvihill,[†] Andrea Tao,[†,||] Peidong Yang,[†] and Jay T. Groves*[,†,§,⊥]

Department of Chemistry, University of California, Berkeley, California 94720, Lawrence Berkeley National Laboratory, Berkeley, California 94720, and Howard Hughes Medical Institute, University of California, Berkeley, California 94720

Received February 18, 2009; Revised Manuscript Received April 10, 2009

ABSTRACT

Detection and characterization of molecular interactions on membrane surfaces is important to biological and pharmacological research. Here, silver nanocubes interfaced with glass-supported model membranes form a label-free sensor that measures protein binding to the membrane. The technique utilizes plasmon resonance scattering of nanocubes, which are chemically coupled to the membrane. In contrast to other plasmonic sensing techniques, this method features simple, solution-based device fabrication and readout. Static and dynamic protein/membrane binding are monitored and quantified.

Metal nanostructures can be used for the label-free optical detection of molecular binding to surfaces. This is due to strong, environmentally sensitive light scattering caused by the localized surface plasmon resonance (LSPR) of electrons at the metal surface.[1] Characteristic LSPR spectra exist for a variety of shapes and configurations of particles,[2−7] and similar to conventional surface plasmon resonance (SPR) spectrometry, the scattering spectra of the nanostructures are dependent upon the refractive index of the surrounding medium, which enables the detection of molecular binding to or near the nanostructure surface.[4,8,9]

An application of the sensing capabilities of metal nanostructures presented here is the detection of protein binding at phospholipid membrane surfaces. Binding can be observed in a simple, potentially multiplexed sensor device with a straightforward readout. The basic sensor considered here consists of cubic silver nanoparticles (∼100 nm, Figure 1a), or "nanocubes," embedded in a glass-supported lipid bilayer membrane. The nanocubes are deposited onto a glass surface, after which they are chemically modified with a self-assembled monolayer (SAM) of alkanethiol. Subsequent exposure of the surface to lipid vesicles results in formation of a continuous lipid membrane covering the nanocubes and the supporting glass substrate, as depicted in Figure 1a. Experimental justification for this proposed structure is provided below. Binding of molecular ligands to their cognate receptors in the membrane alters the scattering spectra of the nanocubes in a quantifiable manner. In this implementation, target binding is measured by peak shifts in the LSPR scattering spectra, which are monitored in real time using a standard benchtop spectrophotometer. In contrast to many examples of nanostructured sensors,[10−12] this design is based on bottom-up chemical self-assembly approaches. Each step of the process, from the chemically mediated growth of silver nanocubes to the deposition of alkanethiols and phospholipids on the surface of metal particles, is a solution-based process; no patterning or lithographic steps are required. These simple and easily produced devices provide data comparable to much more complex SPR instruments.[13]

There is a pronounced need for analytical technology capable of probing molecular interactions in a cell membrane environment. Most biochemical processes involve membranes at some point and, correspondingly, over half of the one hundred best selling marketed drugs target cellular-membrane-associated proteins.[14,15] To address this need, there has been significant interest in supported lipid bilayers,[16−18] which share many of the same properties as cellular membranes. In particular, supported membranes retain lateral fluidity and allow membrane components to rearrange naturally in response to molecular interactions. Furthermore, membrane proteins are notoriously difficult to work with

* Corresponding author, jtgroves@lbl.gov.
[†] Department of Chemistry, University of California.
[‡] Current address: Early Stage Pharmaceutical Development, Genentech, Inc., 1 DNA Way, South San Francisco, CA 94080.
[§] Lawrence Berkeley National Laboratory.
[||] Current address: Institute for Collaborative Biotechnologies, University of California, Santa Barbara, CA 93106.
[⊥] Howard Hughes Medical Institute.

10.1021/nl900513k CCC: $40.75
Published on Web 04/22/2009

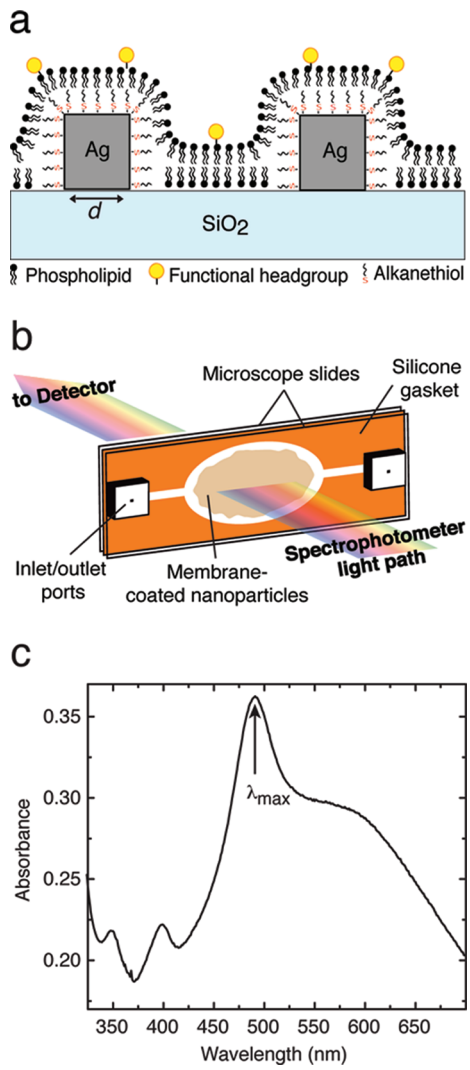

Figure 1. (a) Schematic of nanocubes with edge length *d* embedded in the membrane substrate. A supported bilayer exists over glass, while a hybrid phospholipid/alkanethiol bilayer is over the silver nanocubes. (b) Representation of the flow chamber device used in this work. The device is placed in the light path of a spectrophotometer and allows easy exchange of solution surrounding the substrate. (c) Typical spectrum of a membrane−nanocube substrate, exhibiting the prominent quadripolar LSPR peak, λ_{max}, used to monitor spectral shifts.

outside of the membrane environment; supported membranes offer a strategy to handle these. G-protein coupled receptors provide a case in point and have been screened in a supported membrane microarray format.[19,20] Supported membranes have also been used to reconstitute protein−protein signaling at membrane surfaces[21] and to imitate one face of cell−cell junctions at T-cell synapses.[22,23] The detection strategy presented here takes advantage of the unique optical properties displayed by shaped metal nanocrystals. Silver nanocubes exhibit a sharp quadripolar LSPR peak that provides a sensitive gauge of the refractive index in the immediately surrounding environment and have been characterized both experimentally and theoretically.[6,7,24] At the quadripolar LSPR wavelength, the electromagnetic field exhibits localized hot spots of amplified intensity which extend approximately 10 nm beyond the metal surface, with the field being strongest along the edges and corners of the cube.[24] This results in less influence from solution components when compared with conventional surface plasmon resonance, which has far longer (200 nm) field penetration depths.[25,26] The nanocube LSPR field still extends beyond the approximately 5 nm thickness of the hybrid bilayer[27] to allow probing of binding at the membrane surface.

The construction of the biosensor begins with drying a solution of silver nanocubes onto a glass substrate. The nanocubes are synthesized using the polyol method,[6,28,29] capped with poly(vinylpyrrolidone) (PVP), and stored in ethylene glycol for extended periods of time (up to months) before use. Nanocubes are first washed extensively with ethanol to remove residual synthetic reagents. A small droplet of the colloidal suspension is spread onto a glass microscope slide, which has been previously cleaned in a 1:4 30% H_2O_2:H_2SO_4 mixture of piranha solution (extremely reactive, use caution). The droplet is allowed to dry under a N_2 atmosphere for 10 min; air exposure is minimized to avoid silver oxidation. Slides are then incubated in a hexane solution with 3 mM 1-octanethiol for at least 12 h to form an alkanethiol SAM over the metal. The slides are subsequently rinsed by immersion in acetone, 2-propanol, and twice in deionized water. After drying under N_2 for 30 min, the nanoparticle-covered slides are assembled into a flow chamber using a silicone gasket (Invitrogen) and a second slide with holes cut to allow solution exchange within the device (Figure 1b). Measurements are conducted using regions of substrates with nanocube densities of approximately 10−100 μm^{-2}, as estimated by darkfield microscopy.

The extinction spectrum of a nanocube-decorated substrate, as monitored by a standard spectrophotometer (Cary 100), is illustrated in Figure 1c. The spectrum is dominated by a large peak with a maximum at λ_{max} corresponding to the quadripolar LSPR of the nanocubes.[6] At these densities, some nanocubes interact to form aggregates that appear as brighter spots by darkfield microscopy (not shown) and in fluorescence images following coating by lipid membranes containing fluorophores for characterization (discussed below and shown in Figure 2a). The large area illuminated by the spectrophotometer (~0.5 cm^2) averages the response from ~10^8 to 10^9 nanocubes, with many apparently remaining as singular particles as judged by the aggregate extinction spectrum. The resulting integrated signal from the ensemble of nanocubes may reduce absolute sensitivity compared with individual particle scattering spectra, as has been argued,[30] but it greatly simplifies the comparison of different substrate preparations, since ensemble averages are far more consistent than the individual particle properties. This latter point proves enabling in the present application.

It is possible to directly measure the response of SAM-coated nanocubes to changes in the surrounding refractive index (RI) by exposing the sensor to aqueous solutions of glycerol and tracking the shift in position of λ_{max} relative to its initial wavelength in water alone. A plot of the shift of the peak versus the refractive index of the surrounding glycerol/water solution yields a sensitivity of 165 nm RI^{-1} (supplementary Figure 1 in Supporting Information). This

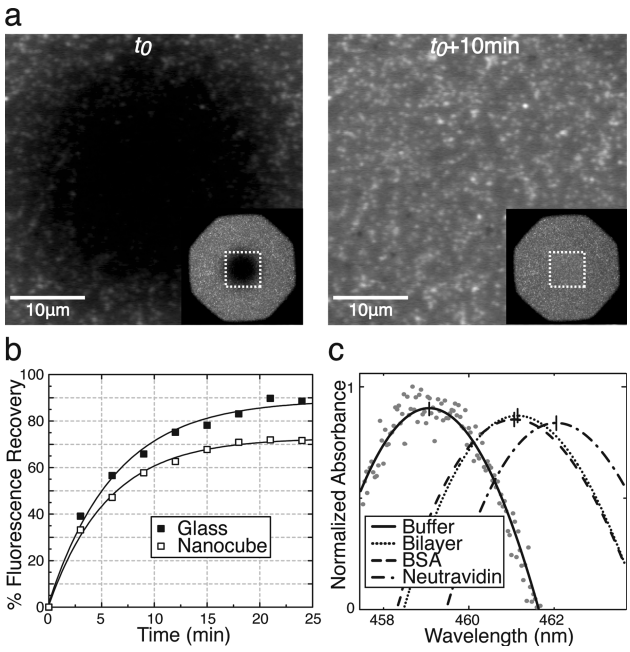

Figure 2. (a) Fluorescence recovery after photobleaching (FRAP) experiment of a nanocube−membrane substrate. The lipids bleached by intense illumination in the microscope as seen at t_0 diffuse away, restoring the intensity over both supported and hybrid bilayer regions. Inset shows a wider view with the magnified region highlighted. (b) Normalized fluorescence recovery of lipids over a nanocube or over glass. An immobile fraction of lipids and limited observation time account for the less than full recovery. Glass and nanocube regions recover exponentially (black lines) with half-lives of 5.6 and 6.3 min, respectively. (c) Peak shift of lipid-coated nanocubes. Polynomial fits of the quadripolar peak of the substrates in buffer before coating by lipids (solid line, with raw data shown as gray dots) and after addition of vesicles containing biotinylated lipids and formation of bilayer/hybrid bilayer on the substrate (dashed line). The substrate is then exposed to 0.03 mg mL^{-1} bovine serum albumin, resulting in virtually no shift (dotted line). The addition of neutravidin, however, causes a substantial peak shift as the protein binds to biotinylated lipids (dot/dash line). Small vertical marks on the spectra denote the peak maximum (λ_{max}) of each curve.

is comparable to the ∼180−220 nm RI^{-1} sensitivity reported for nanometric holes filled with lipid vesicles in a metal film on glass,[31] though less than that of microfabricated metal nanostructures directly interacting with the solvent.[11] It is likely that further optimization of nanocube homogeneity and deposition procedures can increase the observed value. Also, since the evanescent field surrounding the nanocube decays strongly with distance, some of the potential sensitivity of the nanocube substrates may be lost due to the alkanethiol/phospholipid coating. Indeed, shorter chain length alkanethiol SAMs yield larger peak shifts in response to coating by lipids (supplementary Figure 2 in Supporting Information) as described below. The focused sensitivity is, however, an advantage when the actual targets for sensing are molecular monolayers.

To form a phospholipid membrane on the nanocube-coated substrate, the flow chamber is filled with 50 mM Tris, 200 mM NaCl, and pH 7.5 buffer allowed to incubate for 30 min before rinsing with further buffer to remove loosely adhered particles. A solution of lipid vesicles is injected into the flow chamber in the Tris buffer and allowed to incubate for an additional 30 min (shorter incubations than these are also likely sufficient). During this time, vesicles rupture to form a supported phospholipid bilayer over the bare glass regions and a phospholipid monolayer over the alkanethiol-modified nanocubes (supplementary Figure 3 in Supporting Information). The bilayer and monolayer portions of the membrane are continuous, since lipids diffuse freely over the entire substrate as verified by experimental observations described below. This structure is similar to that of other hybrid bilayer membrane systems.[32−34] Excess vesicles remaining on the substrate are washed away with several milliliters of 25 mM Tris, 100 mM NaCl, pH 7.5 buffer. The vesicles consist primarily of 1,2-dioleoylphophotadylcholine (DOPC) along with 0.5 mol % Texas Red 1,2-dihexadecanoyl-*sn*-glycero-3-phosphoethanolamine (TR-DHPE, for fluorescence imaging) as well as 10 mol % of (DOGS-NTA-Ni) or 3 mol % 1,2-dipalmitoyl-*sn*-glycero-3-phosphoethanolamine-*N*-(biotinyl) (biotin-PE) as indicated (TR-DHPE from Invitrogen; all others from Avanti Polar Lipids). Vesicles are prepared by drying lipids dissolved in $CHCl_3$ in a round-bottom flask, suspending the dried lipid film in water, and repeatedly passing the suspension through a 100 nm pore filter in a high pressure extruder at 50 °C.

Coating the nanocubes with an alkanethiol SAM is required to create a laterally fluid, continuous membrane over the glass and metal substrate surface. This is demonstrated by FRAP experiments, where fluorophores in a small region of the substrate surface are bleached under high intensity illumination in a microscope and recover with time due to the lateral diffusion of membrane components (Figure 2a). The nanocubes are clearly visible in the fluorescence images due to fluorescence enhancement, discussed below. Notably, when the nanocubes are functionalized with alkanethiol prior to formation of the supported bilayer, these enhanced regions of fluorescence bleach and recover in the same time scale as the bulk of the supported membrane. This confirms that lipids in the range of the nanocube surface plasmon are diffusively connected to the rest of the membrane (Figure 2b). When the nanocubes are not functionalized with alkanethiol SAMs, the surface and initial (t_0) FRAP images look qualitatively the same by microscopy, but the fluorescence of the nanocubes does not recover with time (supplementary Figure 4 in Supporting Information). This illustrates that the lipid material on nanocubes that remain uncoated by an alkanethiol SAM is not continuous with the surrounding bilayer medium. Similar phenomena are well-known in patterned metal/glass surfaces and have been used as a method of patterning lipid membranes.[35,36] The observation that nanocubes without SAM coating do produce fluorescence enhancement but do not recover provides confirmatory evidence that the enhancement seen from SAM-coated nanocubes is resulting from lipids on the nanocube itself and not the surrounding bilayer. The schematic sketch in Figure 1 is based on this experimental evidence. It should also be noted that defects in the membrane are sure to exist; we know only that they are of insufficient density to significantly interfere with long-range diffusive transport.

The nanocubes are seen clearly in fluorescence microscopy images as objects that appear brighter than the surrounding fluorescent supported bilayer (Figure 2a). There are several potential causes for the high relative fluorescence intensity. Nanocubes provide an excess of local surface area compared to the flat substrate. However, the nanocubes are approximately 4-fold brighter than would be expected based purely on the geometry of a monolayer-coated 100 nm cube (see supplementary note in Supporting Information). One explanation for this is that it is possible for fluorophores to energetically couple to nearby plasmonic fields, resulting in a localized enhancement of fluorescence intensity, even for fluorophores without good spectral overlap between their excitation spectrum and the plasmonic scattering profile.[37,38] Another possible contributor to the increased intensity is high local concentrations of lipidated fluorophores induced by the metal surface potential, the high local curvature of the membrane on the nanocube, and differences in lipid surface density, as is observed in other membrane systems.[39] All these factors may exist simultaneously but are not distinguishable here and do not affect the sensing technique, which is not fluorescence-based.

To measure small shifts in the LSPR-derived absorbance spectrum of the sensor resulting from molecular binding, the quadripolar absorbance peak is fit to a fifth order polynomial function over a consistent sampling range. This allows the precise determination of peak maximum position, and in the present implementation at least 0.02 nm resolution is achieved, as discussed below. In contrast to previous examples of this approach, changes in the peak maximum position (λ_{max}, Figure 1c) are monitored rather than changes in the peak centroid position[40] or its absorbance,[41] both of which give less consistent data here. This is partly because the arrays of nanoparticles are randomly ordered, and the density of particles can vary from one array to another as well as on a single substrate. The resulting variance in particle density has a greater impact on the absolute absorbance of the quadripolar peak than its position, and considering peak position alone allows for simpler comparisons between sensor substrates.

The level of nonspecific binding to the membrane−nanocube substrates is extremely low compared with some previous reports of LSPR-based membrane binding sensors.[3] As seen in Figure 2c, coating an alkanethiol-modified nanocube substrate with phospholipids (96.5% DOPC, 3% biotin-cap-PE, 0.5% TR-DHPE) results in a 2.40 nm shift in the quadripolar peak. Subsequent addition of 0.03 mg mL^{-1} bovine serum albumin barely shifts the peak position by a further 0.03 nm. Conversely, the addition of neutravidin, which specifically binds to biotin-headgroup lipids incorporated into this membrane composition, results in a 1.26 nm shift. This constitutes a signal/noise ratio of 42 over nonspecific binding.

Molecular binding to the membrane surface can also be monitored dynamically, enabling kinetic analyses. In the example considered here, DOGS-NTA-Ni lipids provide the binding functionality—a membrane receptor for these purposes—in a membrane mixture of 89.5% DOPC, 10% DOGS-NTA-Ni, and 0.5% TR-DHPE. The DOGS-NTA-Ni lipids bind to a hexahistidine tag at the C-terminus of yellow fluorescent protein (YFP).[42] Other membrane-associated species including membrane proteins, DNA/RNA, or lipid-conjugated small molecules can also be readily used in this configuration.[43−45] The graph in Figure 3 (dark squares) shows the shift in the LSPR peak position, λ_{max}, as YFP unbinds from a DOGS-NTA-Ni functionalized membrane. The LSPR shift is directly related to protein density (right axis) by the fluorescence of YFP, as discussed below. The unbinding follows a biexponential decay with half-lives of 6.3 ± 0.3 and 320 ± 40 min, measured by the shift in LSPR peak position. The error reported for these and similar desorption fits is determined by the uncertainty of a least-squares fit to a biexponential decay model performed in OriginPro (OriginLabs). These results are consistent with previous characterizations of protein/DOGS-NTA-Ni membrane binding which show that polyhistidine-tagged proteins exist in both loosely bound and tightly bound states. The two binding states result in two characteristic desorption time scales, the shorter of which is independent of DOGS-NTA-Ni density and has previously been measured to be ~6 min for other hexahistidine proteins.[46] In the absence of DOGS-NTA-Ni lipids, the supported membrane strongly resists nonspecific adsorption of the YFP protein and no substantial peak shift is seen (Figure 3, open squares). The time resolution of these kinetic measurements is determined only by the acquisition rate of the spectrophotometer. In this case it is ~50 s per spectrum, but much faster rates are possible, since the scattering-based readout means one may simply raise illumination intensity to increase signal strength and acquisition speed.

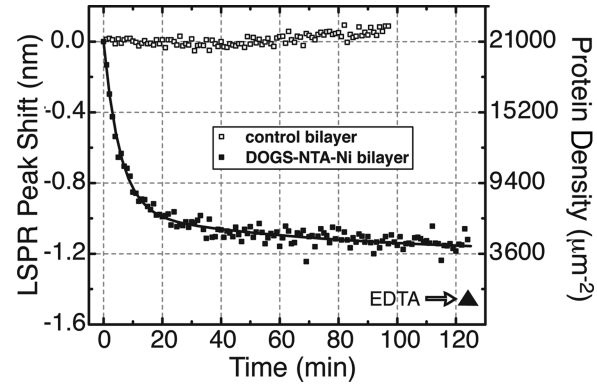

Figure 3. YFP unbinding monitored by LSPR peak shift. Observed shift in λ_{max} position compared with $t = 0$ for a nanocube-embedded bilayer with (dark squares) or without (open squares) DOGS-NTA-Ni lipids. The line is a least-squares fit of the equation $y = A \exp[-t/a] + B \exp[-t/b] + y_0$ to the data where y is the shift in λ_{max} and t is time. The indicated triangle denotes the observed peak shift upon addition of EDTA, which removes all remaining YFP and defines y_0. The remaining terms are found by the fitting procedure. The right-hand axis is the calculated protein density by considering the fluorescence of YFP bound to identical bilayers as outlined in the text.

The LSPR-based measurements are compared to fluorescence from YFP on the membrane surface, which is directly monitored by microscopy in a glass-bottomed 96 well plate format (Nalge-Nunc). This configuration is chosen to com-

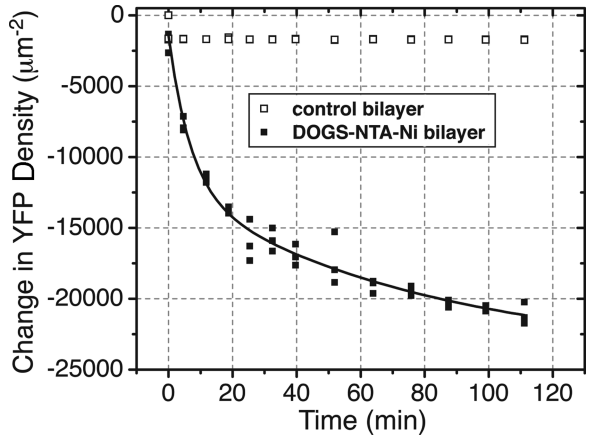

Figure 4. Change in YFP density monitored by fluorescence. Observed change in density of YFP on bilayers with (dark squares) or without (open squares) DOGS-NTA-Ni headgroup lipids. The line represents a fit as in Figure 3, with y_0 corresponding to a decrease in YFP density ($-21000\ \mu m^{-2}$) resulting in loss of all bound protein.

pare the data from the nanocube hybrid membranes to conventional supported membranes without nanocubes. Membranes are of the same compositions as those used with the LSPR measurements and are formed similarly as described elsewhere.[46] After samples are loaded with YFP, fluorescence microscopy images are taken of different regions of several replicate bilayers over the course of time, with manual rinsing of wells between each image acquisition (Nikon TE-300 equipped with a high-pressure Hg lamp and Chroma 31001 filter set). The intensity of the fluorescence microscopy images is proportional to the amount of YFP on the surface. These data show that YFP desorbs from the membrane biexponentially with half-lives of 7 ± 1 and 80 ± 8 min^{-1} (Figure 4), which essentially agrees with the LSPR-based measurements. Variation in the longer half-lives may result from the slightly different experimental configurations used for experimental convenience.

The fluorescence microscopy images used above also provide a direct way to estimate the amount of protein bound to the membrane, and thus the sensitivity of the LSPR assay. The absolute surface density of protein can be measured using a set of bilayer calibration standards containing varying concentrations of BODIPY-DHPE lipid (Invitrogen), which provide the relationship between fluorescence intensity and surface density of fluorophore. The intensity of YFP can be scaled to be directly comparable to that of BODIPY-DHPE, which allows the density of YFP to be inferred.[47] This analysis shows that initial protein density on the bilayer is approximately 21000 μm^{-2} and decreases over the course of the experiment to approximately 2000 μm^{-2} (Figure 4). Since the membranes for fluorescence and LSPR measurements are the same, the fluorescence quantification may be used for the protein density scale in Figure 3. This direct mapping is further supported by the similar desorption kinetics of two membranes (supplementary Figure 5 in Supporting Information) and illustrates that the LSPR sensor can read out a wide range of bound protein densities. Thus, if properly calibrated, LSPR measurements provide a quantitative measurement of protein on the sensor surface. In this case, the change in protein density corresponds to a change in mass of 120 ng cm^{-2} and a response factor of approximately 170 nm cm^2 ng^{-1} for the LSPR measurements. Replicate sensor substrates made with the same batch of nanocubes have similar sensitivities.

An estimate of sensor noise is found by considering data from the negative control bilayer (without DOGS-NTA-Ni), shown in Figure 3 (open squares), where protein binding to the membrane does not occur. The first 60 measurements have a standard deviation of 0.02 nm, which corresponds to a mass density of 1.5 ng cm^{-2} by applying the sensitivity of 170 nm cm^2 ng^{-1}. This also results in a calculated limit of detection ($3\times$ noise)[48] of 4.5 ng cm^{-2}. The 0.02 nm value also provides an upper limit to the noise of the polynomial peak fitting method described above—the true resolution is likely much finer. While the limit of detection of supported bilayers formed in microfabricated nanoscale holes in metal films on glass is reported to be 0.1 ng cm^{-2},[41] the numbers quoted for the nanocube membrane sensor here represent an unoptimized initial observation that is likely to be surpassed by further sensor development. Fundamentally the underlying optical physics is the same, so similar sensitivities are likely achievable in all formats.

Many implementations of nanostructure-based sensors require complicated nanostructured templates and device fabrication. Realization of this sensor only requires simple-to-manufacture, self-assembled nanocube/bilayer detection surfaces, along with a standard absorbance spectrophotometer. The membrane-coated nanocube substrates are also potentially very easy to multiplex. Rather than a dedicated flow chamber as used here, it should be possible to realize the same basic system using glass-bottomed 96 well plates and an optical plate reader (e.g., high-resolution models from Molecular Devices, BMGLabtech, and Biotek, among others). This allows easy multiplexing and scalability of the technique, since nanocube deposition, modification, and membrane coating could all be performed in an individual well whose spectrum is read out independently and analyzed as above. The membrane functionality of this technique allows readout of binding in an environment very different than that in solution or provided in most standard SPR formats. Some applications may not require the membrane environment itself, but membrane resistance to nonspecific binding (especially of proteins) may still prove useful as a scaffold for monitoring natively soluble proteins interacting with each other.

Acknowledgment. This work was supported by the Chemical Sciences, Geosciences, and Biosciences Division, Office of Basic Energy Sciences, U.S. Department of Energy under Contract Number DE-AC03-76SF00098 and NIH.

Supporting Information Available: Supporting figures and note. This material is available free of charge via the Internet at http://pubs.acs.org.

References

(1) Willets, K. A.; Van Duyne, R. P. *Annu. Rev. Phys. Chem.* **2007**, *58*, 267–297.
(2) Kelly, K.; Coronado, E.; Zhao, L.; Schatz, G. *J. Phys. Chem. B* **2003**, *107*, 668–677.

(3) Baciu, C. L.; Becker, J.; Janshoff, A.; Sonnichsen, C. *Nano Lett.* **2008**, *8*, 1724–1728.
(4) Yonzon, C. R.; Jeoungf, E.; Zou, S. L.; Schatz, G. C.; Mrksich, M.; Van Duyne, R. P. *J. Am. Chem. Soc.* **2004**, *126*, 12669–12676.
(5) Prikulis, J.; Hanarp, P.; Olofsson, L.; Sutherland, D.; Kall, M. *Nano Lett.* **2004**, *4*, 1003–1007.
(6) Tao, A.; Sinsermsuksakul, P.; Yang, P. D. *Angew. Chem., Int. Ed.* **2006**, *45*, 4597–4601.
(7) Tao, A.; Sinsermsuksakul, P.; Yang, P. *Nat. Nanotechnol.* **2007**, *2*, 435–440.
(8) Haes, A.; Chang, L.; Klein, W.; VanDuyne, R. *J. Am. Chem. Soc.* **2005**, *127*, 2264–2271.
(9) Zhao, J.; Das, A.; Zhang, X.; Schatz, G.; Sligar, S.; VanDuyne, R. *J. Am. Chem. Soc.* **2006**, *128*, 11004–11005.
(10) Haes, A. J.; Zou, S. L.; Schatz, G. C.; Van Duyne, R. P. *J. Phys. Chem. B* **2004**, *108*, 6961–6968.
(11) Hicks, E. M.; Zhang, X.; Zou, S.; Lyandres, O.; Spears, K. G.; Schatz, G. C.; Van Duyne, R. P. *J. Phys. Chem. B* **2005**, *109*, 22351–22358.
(12) Rindzevicius, T.; Alaverdyan, Y.; Dahlin, A.; Hook, F.; Sutherland, D. S.; Kall, M. *Nano Lett.* **2005**, *5*, 2335–2339.
(13) *Handbook of surface plasmon resonance*; Schasfoort, R. B., Tudos, A. J., Eds.; Royal Society of Chemistry: Cambridge, 2008.
(14) Drews, J. *Science* **2000**, *287*, 1960–1964.
(15) Yildirim, M. A.; Goh, K.-I.; Cusick, M. E.; Barabasi, A.-L.; Vidal, M. *Nat. Biotechnol.* **2007**, *25*, 1119–1126.
(16) Sackmann, E. *Science* **1996**, *271*, 43–48.
(17) Groves, J. T. *Curr. Opin. Drug Discovery Dev.* **2002**, *5*, 606–612.
(18) Tanaka, M.; Sackmann, E. *Nature (London)* **2005**, *437*, 656–663.
(19) Bieri, C.; Ernst, O. P.; Heyse, S.; Hofmann, K. P.; Vogel, H. *Nat. Biotechnol.* **1999**, *17*, 1105–1108.
(20) Fang, Y.; Frutos, A. G.; Lahiri, J. *ChemBioChem* **2002**, *3*, 987–991.
(21) Gureasko, J.; Galush, W. J.; Boykevisch, S.; Sondermann, H.; Bar-Sagi, D.; Groves, J. T.; Kuriyan, J. *Nat. Struct. Mol. Biol.* **2008**, *15*, 452–461.
(22) Groves, J. T.; Dustin, M. L. *J. Immunol. Methods* **2003**, *278*, 19–32.
(23) Mossman, K. D.; Campi, G.; Groves, J. T.; Dustin, M. L. *Science* **2005**, *310*, 1191–1193.
(24) Sherry, L. J.; Chang, S. H.; Schatz, G. C.; Van Duyne, R. P.; Wiley, B. J.; Xia, Y. N. *Nano Lett.* **2005**, *5*, 2034–2038.
(25) Jung, L.; Campbell, C.; Chinowsky, T.; Mar, M.; Yee, S. *Langmuir* **1998**, *14*, 5636–5648.
(26) Zhou, Y.; Xu, H.; Dahlin, A. B.; Vallkil, J.; Borrebaeck, C. A. K.; Wingren, C.; Liedberg, B.; Hook, F. *Biointerphases* **2007**, *2*, 6–15.
(27) Leonenko, Z. V.; Finot, E.; Ma, H.; Dahms, T. E. S.; Cramb, D. T. *Biophys. J.* **2004**, *86*, 3783–3793.
(28) Fievet, F.; Lagier, J. P.; Blin, B.; Beaudoin, B.; Figlarz, M. *Solid State Ionics* **1989**, *32−33*, 198-–205.
(29) Sun, Y.; Xia, Y. *Science* **2002**, *298*, 2176–2179.
(30) Anker, J. N.; Hall, W. P.; Lyandres, O.; Shah, N. C.; Zhao, J.; Van Duyne, R. P. *Nat. Mater.* **2008**, *7*, 442–453.
(31) Dahlin, A. B.; Jonsson, M. P.; Hook, F. *Adv. Mater.* **2008**, *20*, 1436-+.
(32) Meuse, C. W.; Niaura, G.; Lewis, M. L.; Plant, A. L. *Langmuir* **1998**, *14*, 1604–1611.
(33) Kastl, K.; Ross, M.; Gerke, V.; Steinem, C. *Biochemistry* **2002**, *41*, 10087–10094.
(34) Jackson, B. L.; Nye, J. A.; Groves, J. T. *Langmuir* **2008**, *24*, 6189–6193.
(35) Groves, J. T.; Ulman, N.; Boxer, S. G. *Science* **1997**, *275*, 651–653.
(36) Groves, J. T.; Ulman, N.; Cremer, P. S.; Boxer, S. G. *Langmuir* **1998**, *14*, 3347–3350.
(37) Haes, A.; Zou, S.; Zhao, J.; Schatz, G.; VanDuyne, R. *J. Am. Chem. Soc.* **2006**, *128*, 10905–10914.
(38) Zhang, J.; Fu, Y.; Chowdhury, M. H.; Lakowicz, J. R. *J. Phys. Chem. C* **2008**, *112*, 9172–9180.
(39) Sanii, B.; Parikh, A. N. *Soft Matter* **2007**, *3*, 974–977.
(40) Nenninger, G. G.; Piliarik, M.; Homola, J. *Meas. Sci. Technol.* **2002**, *13*, 2038–2046.
(41) Dahlin, A. B.; Tegenfeldt, J. O.; Hook, F. *Anal. Chem.* **2006**, *78*, 4416–4423.
(42) Ormö, M.; Cubitt, A. B.; Kallio, K.; Gross, L. A.; Tsien, R. Y.; Remington, S. J. *Science* **1996**, *273*, 1392–1395.
(43) Salafsky, J.; Groves, J. T.; Boxer, S. G. *Biochemistry* **1996**, *35*, 14773–14781.
(44) Yoshina-Ishii, C.; Boxer, S. G. *J. Am. Chem. Soc.* **2003**, *125*, 3696–3697.
(45) Parthasarathy, R.; Groves, J. T. *Proc. Natl. Acad. Sci. U.S.A.* **2004**, *101*, 12798–12803.
(46) Nye, J. A.; Groves, J. T. *Langmuir* **2008**, *24*, 4145–4149.
(47) Galush, W. J.; Nye, J. A.; Groves, J. T. *Biophys. J.* **2008**, *95*, 2512–2519.
(48) Homola, J. *Chem. Rev.* **2008**, *108*, 462–493.

NL900513K